An Acad Bras Cienc (2022) 94(3): e20210917 DOI 10.1590/0001-3765202220210917
Anais da Academia Brasileira de Ciências | *Annals of the Brazilian Academy of Sciences*
Printed ISSN 0001-3765 I Online ISSN 1678-2690
www.scielo.br/aabc | www.fb.com/aabcjournal

CHEMICAL SCIENCES

Magnetic alignment of rhodamine/magnetite dual-labeled microtubules probed with inverted fluorescence microscopy

HENRIQUE EISI TOMA, DANIEL OLIVEIRA & FERNANDO M. DE MELO

Abstract: Molecular machines, as exemplified by the kinesin and microtubule system, are responsible for molecular transport in cells. The monitoring of the cellular machinery has attracted much attention in recent years, requiring sophisticated techniques such as optical tweezers, and dark field hyperspectral and fluorescence microscopies. It also demands suitable procedures for immobilization and labeling with functional agents such as dyes, plasmonic nanoparticles and quantum dots. In this work, microtubules were co-polymerized by incubating a tubulin mix consisting of 7 biotinylated tubulin to 3 rhodamine tubulin. Rhodamine provided the fluorescent tag, while biotin was the anchoring group for receiving streptavidin containing species. To control the microtubule alignment and consequently, the molecular gliding directions, functionalized iron oxide nanoparticles were employed in the presence of an external magnet field. Such iron oxide nanoparticles, (MagNPs) were previously coated with silica and (3-aminopro-pyl) triethoxysilane (APTS) and then modified with streptavidin (SA) for linking to the biotin-functionalized microtubules. In this way, the binding has been successfully performed, and the magnetic alignment probed by Inverted Fluorescence Microscopy. The proposed strategy has proved promising, as tested with one of the most important biological structures of the cellular machinery.

Key words: Molecular machines, kinesin and microtubules, magnetic nanoparticles, fluorescence microscopy, CytoViva hypermicroscopy.

INTRODUCTION

Protein machines, also referred to as molecular motors, are the origin of nearly all biological movements within a eukaryotic cell. Conversion of chemical energy into mechanical work, harnessed by the hydrolysis of ATP, propels the protein machines along a cytoplasmic system of fibers, known as microtubules. These species are naturally occurring, filamentous fibers made up of α- and β-tubulin globular protein monomers. During the motion of the transporting molecules in the cell's cytoskeleton, tubulin polymerizes, yielding relatively straight hollow tubes with an outer diameter of approximately 25 nm and tens of a micrometer in length. Their malfunctioning and instability have already been associated with Alzheimer's disease and cancer (Rath & Kozielski 2012).

Kinesin is a well-known naturally occurring molecular machine capable of unidirectional cargo transport upon microtubule interaction, and consequently, is an attractive candidate as a constituent of synthetic molecular machines. Kinesin moves along a microtubule within the cytoskeletal network, having several functions, including synapse activity (Vale & Milligan 2000), (Dixit et al. 2008). Efforts have been addressed to engineer tailor-made artificial nanotransport systems to carry out directional transport of

nanoobjects (Bachand et al. 2004), (Bohm et al. 2001). In a typical design, ATP-fueled kinesin motor proteins are immobilized on a glass surface while microtubules loaded with cargo are propelled over the motors. Alternatively, molecular shuttles can be assembled mimicking the natural cells intracellular transport mechanism where the kinesin protein moves over microtubules tracks. (Verhey et al. 2011), (Du et al. 2005), (Keya et al. 2020), (Smith et al. 2010). From a device engineering perspective, the latter approach for molecular shuttles is more appealing since multiple microtubules tracks with varying directions can be designed in the same device; moreover, bidirectional cargo transport can be achieved on the same track if different motor proteins are used (e.g., kinesin and dynein). Kinesin motors have, in fact, been successfully used for many applications such as biomedical sensors (Fischer et al. 2009), biomolecular motion (van den Heuvel & Dekker 2007), and nanoparticle transport (Doot et al. 2007), (Oliveira et al. 2012).

Harnessing the unique properties of the kinesin/microtubule pair will set the stage for the development of functional micro- and nanoscale biodevices. Whether devices are to be fabricated with the configuration where kinesin protein are transported along microtubule tracks, or the reverse configuration, one major challenge is to control the microtubule alignment and orientation over a long-range order. To date, several strategies have been studied to address such challenge, for instance, by using complex lithographic techniques (Moorjani et al. 2003), or utilizing viscous fluid forces (Brown & Hancock 2002). However, such approaches involve high cost and exhibit technical limitations, since the alignment distance will be limited by microtubule length.

By focusing on the individual scale, molecular machines can be suitably monitored with optical tweezers, based on the transference of the optical angular momentum (optical torque) to the microsphere center of mass, when it is not perfectly aligned along the beam symmetry axis (Diniz et al. 2019). This technique has also been successfully employed in the study of cell membranes and their tunneling nanotubes (Nussenzveig 2018, 2019).

On a collective scale, the monitoring of the cellular machinery can be greatly facilitated by using nanoparticles attached to the tubulins outer surface. Previously, our group has shown that quantum dots and gold nanoparticles can be anchored to the microtubule surface, by selective binding (Oliveira et al. 2018a, b) facilitating their monitoring by fluorescence and plasmonic effects, respectively.

The binding of superparamagnetic iron oxide nanoparticles provides another interesting possibility to be explored, especially because of the possibility to exert some magnetic control of the microtubule dynamics. Although, to the best of our knowledge, the application of modified ferrite nanoparticles in molecular machinery is mostly scarce to the present time (Inaba et al. 2020), (Hutchins et al. 2007), (Platt et al. 2005), it should be mentioned that superparamagnetic nanoparticles are present in biological systems, especially in the so called magnetosomes. They are found in magnetotactic bacteria, which usually contain 15 to 20 magnetite crystals aligned in a chain enclosed by a lipid bilayer membrane. Because of this arrangement, they respond to the geomagnetic fields like a compass needle (Pósfai et al. 2013). Magnetic particles are also found in magnetotactic algae and even in human brain (Kirchwinck 1994), but their function is not yet well understood. It should also be mentioned the pioneering work of F. Crick in investigating the physics of cytoplasm using magnetic nanoparticles (Crick 1950). Nowadays, iron oxide nanoparticles are being widely

employed in medical applications ksuch as drug delivery (Vangijzegem et al. 2019), hyperthermal therapy (Vauthier et al. 2011), imaging (Melo et al. 2018, 2021) and NMR contrasting agents (Da Silva et al. 2016), (Uchiyama et al. 2015).

Relying on strong and specific interactions (e.g., biotin-streptavidin) microtubules can be coupled to functionalized nanocrystals, and accordingly, the interaction of such a complex can be visualized and investigated. This being the case, it is anticipated that molecular shuttles can be engineered by manipulating not only the cargo to be transported by kinesin but also the microtubule track network, and vice-versa. Since various biomolecules can be covalently derivatized with biotin, a magnetic affinity probe may be fabricated by coupling biotinylated capturing probe to streptavidin-based iron oxide nanoparticles. SA is a non-glycosylated protein capable of binding biotin or biotinylated molecule with extremely high affinity (Oladipo et al. 2007), (Katrukha et al. 2017).

Accordingly, in this work we first co-polymerized the microtubules by incubating a tubulin mix consisting of 7 biotinylated tubulin to 3 rhodamine tubulin. Rhodamine provides the fluorescent tag, while biotin is the anchoring group for receiving SA containing species. Then we carried out the synthesis and functionalization of iron oxide nanoparticles, MagNPs, with silica and APTS, for their subsequent modification with SA. The magnetic alignment was investigated using an Inverted Fluorescence Microscope, and the system characterization was carried out utilizing Electron Microscopy, X-Ray Fluorescence Spectroscopy, Infrared Spectroscopy and Vibrating Sample Magnetometer

MATERIALS AND METHODS

Chemicals

All materials and chemicals were used as supplied. Ethylene glycol, glycerol, bis(2-aminoethylether)-*N*,*N*,*N*',*N*'-tetraacetic acid (EGTA), piperazine-*N*,*N*''-bis(2-ethanesulfonic acid) (PIPES), ATP, 1,4-dithiothreitol (DTT), NaOH, magnesium chloride, glycerol, paclitaxel (taxol), polysorbate 20 (Tween 20), guanosine 5'-triphosphate (GTP), Glycine-HCl, glucose oxidase, catalase, glucose, phosphate buffered saline (PBS), BRB80 buffer, tetraethyltriethoxysilane (TEOS), (3-aminopropyl)triethoxysilane (APTS), glacial acetic acid were purchased from Sigma-Aldrich, São Paulo. Ferrous and ferric chloride were obtained from Vetec Co, São Paulo.

Kinesin, tubulin (porcine brain), tubulin (biotin conjugate; porcine brain) and tubulin (rhodamine conjugate; porcine brain) were purchased from Cytoskeleton Inc. (Denver, CO, USA). The lyophilized kinesin protein was reconstituted at 5 mg/mL in a buffer containing 100 mM PIPES, 200 mM KCl, 2 mM $MgCl_2$, 1 mM DTT and 20 µM ATP, pH 7.0. 1 µL aliquots of reconstituted protein were snap-frozen in liquid nitrogen and stored at -70 °C. Porcine tubulin proteins, all 3 variations (unlabeled, rhodamine-labeled and biotin-labeled), were reconstituted to a final concentration of 50 µM in BRB80 buffer (80 mM PIPES, 1 mM EGTA, 1 mM $MgCl_2$, pH 6.9) containing 1 mM GTP (guanosine triphosphate) and 5% glycerol, divided into 1 µL aliquots and stored at -70 °C. To prepare microtubules, a fresh tubulin aliquot was thawed at 37 °C and allowed to polymerize for 30 minutes, followed by dilution to 0.5 µM with warm BRB80 buffer supplemented with 20 µM taxol. Unlabeled microtubules were polymerized as stated above from porcine tubulin, while rhodamine- and biotin-labeled microtubules were prepared from

a mixture at a ratio of seven unlabeled tubulin to three labeled tubulin.

Streptavidin-based iron oxide nanoparticle synthesis

APTS functionalized iron oxide nanoparticles were prepared by a previously reported method (Yamaura et al. 2004). Briefly, 5 mol L^{-1} NaOH solution was added into a mixed solution of 0.25 mol dm^{-3} ferrous chloride and 0.5 mol dm^{-3} ferric chloride (molar ratio 1:2) until obtaining pH 11 at room temperature. The slurry was washed repeatedly with distilled water. Then particles were magnetically separated from the supernatant and redispersed in aqueous solution at least three times, until obtaining pH 7. After that, the surface of these particles was coated with a silica shell using TEOS (Stober et al. 1968) and APTS.

Generally, the procedure consists of heating the magnetite suspension with glycerol, following by a drop wise addition of 40 ml (10%, v/v) water solution of APTES (pH 4.0, adjusted with glacial acetic acid). Then, the solution is gently stirred for 3 h. In the sequence, the silanized particles are separated magnetically, washed with distilled water and dried. Immobilization of SA on MagNPs was conducted in a two-step reaction using glutaraldehyde as coupling agent. Typically, 10 mg MagNPs were added dropwise into 20 mL of glutaraldehyde solution of 2.5 % (v/v) in 10 mmol.dm^{-3} PBS (pH 7.4) and the suspension was shaken for 2 h under nitrogen atmosphere at room temperature. The obtained aldehyde-based MagNPs were then incubated with SA in PBS after being washed twice with PBS. Figure 1 (a, b) shows a schematic representation of the whole synthesis.

Dual labeled microtubules

Labeling with MagNPs bearing a streptavidin layer was carried out by incubating 20 µL of 0.5 µM rhodamine and biotin co-polymerized microtubules with 20 µL of 2 mg/mL SA-MagNPs solution for 20 minutes. The dual labeled microtubules were then transferred into a flow cell and placed in the fluorescence microscope. A $Nd_2Fe_{14}B$ magnet was placed in the microscope under the flow cell to induce a magnetic field to orient the microtubules.

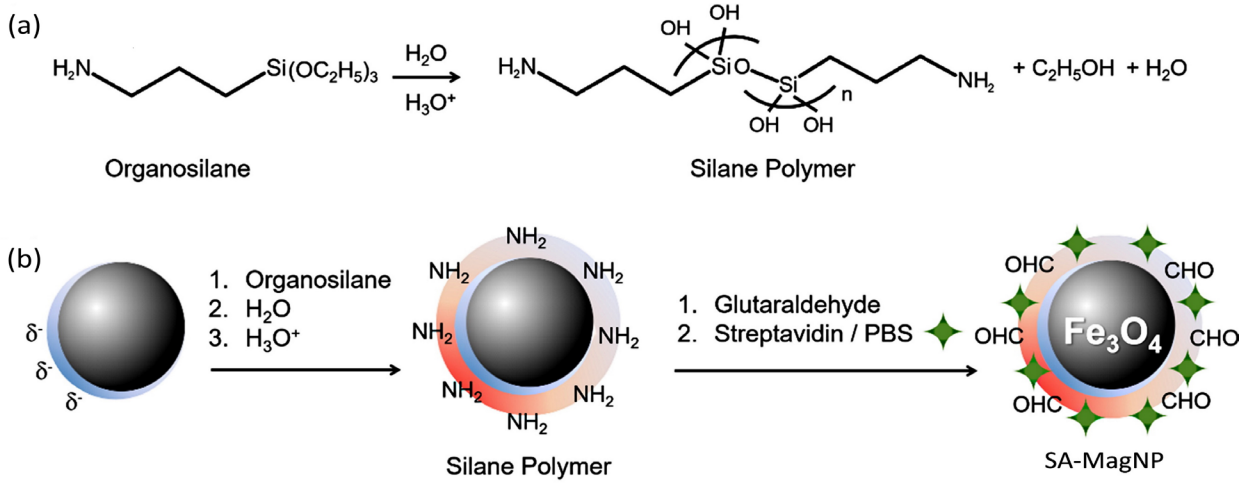

Figure 1. (a) Simplified reaction scheme of hydrolysis and condensation with production of silane polymer with TEOS and APTS, followed by (b) the activation with glutaraldehyde to attach streptavidin.

Fluorescence microscopy

Fluorescent microtubules labeled with SA-MagNPs were visualized on an inverted fluorescence microscope (Axiovert 200, Carl Zeiss) equipped with a Plan-Apo 63x/1.4 NA oil-immersion objective (Figure 2). The number 10 filter set (Carl Zeiss) was used, providing an excitation band pass from 450 to 490 nm and an emission band pass of 515 to 565 nm. Images were recorded on an Axiocam HSm digital camera (Carl Zeiss) and processed using the ZEN software (Carl Zeiss).

Glass surface is the traditional choice for bio-motile systems. The majority of bio-motility research has been demonstrated within a thin glass chamber, the so-called flow cell. When using glass surfaces to study the interaction and motility of the kinesin/microtubule molecular machine, it is essential to treat surfaces with casein protein as a way to passivate the surface and therefore prevent nonspecific interactions between the kinesin protein and microtubules with glass surfaces. Otherwise, the studied protein might become inactivated (Ozeki et al. 2009).

Flow cells were assembled on a microscope NEXTERION® ultra-clean glass B (Schott, using double-sided scotch tape as a spacer. Two pieces of double-sided scotch tape (3M 665 double-sided tape) are placed approximately 6 mm apart from each other on a glass slide. Then, an ultra-clean NEXTERION® glass cover slip (Schott) was placed over the tape channel, resulting in a flow cell with a volume of approximately 10 µL. Once solutions are injected onto the chamber, the flow cell exposed ends were capped with nail polish to prevent evaporation. The standard flow cell used throughout this report is displayed in Figure 2.

Dark-Field CytoViva hyperspectral microscopy

Dark field optical images were obtained with a CytoViva® ultra resolution imaging system, composed by a special arrangement mounted

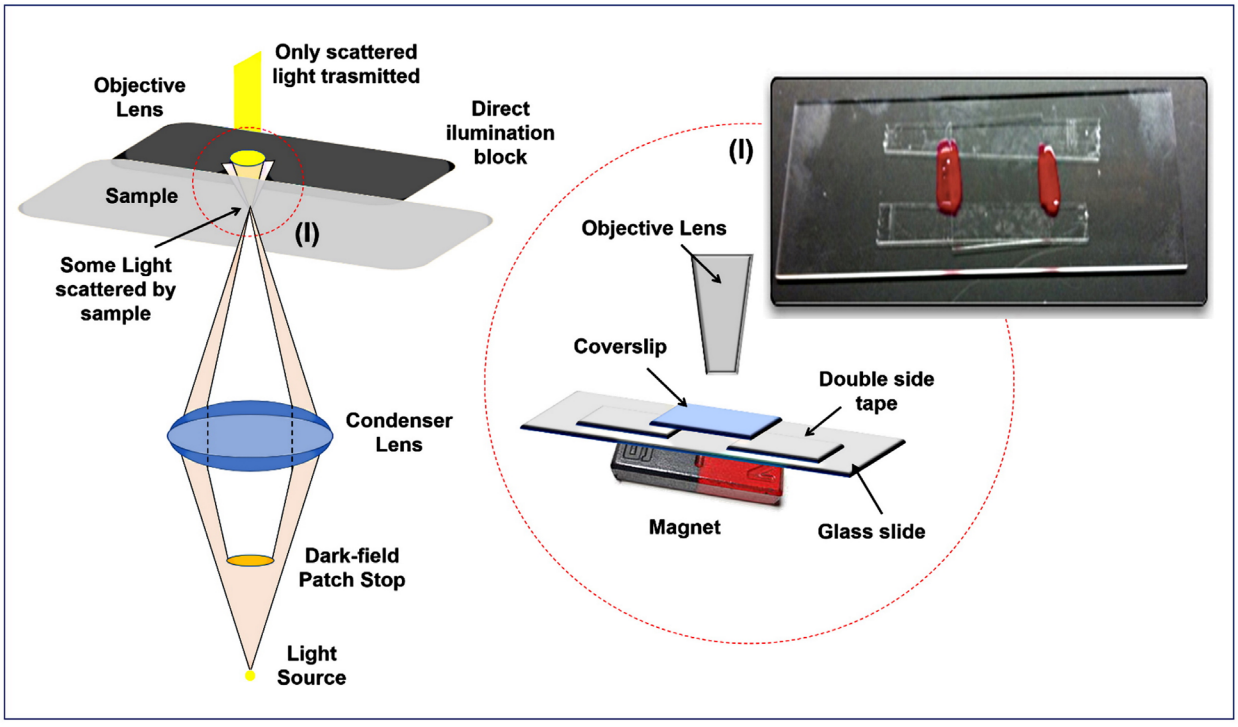

Figure 2. Experimental setup for the inverted fluorescence microscope and the flow cell arrangement.

on an Olympus BX51 microscope, encompassing suitable detection for recording the single particles Rayleigh scattering spectra. In the dark-field configuration, a hollow light cone is generated and focused on the specimen. In this arrangement, only the light scattered and diffracted inside the cone can reach the objective, which has a numerical aperture smaller than the numerical aperture of the dark-field condenser. Since the zero-order diffracted light is not collected, the particles appear as bright spots on a dark background. The resolution power is limited by the light diffraction. The CytoViva® system uses an annular cardoid condenser (Vainrub et al. 2006) with high annular aperture that enables the collection of higher order diffracted light by the objective, rising the resolution power to λ/5. The sample was prepared by drop casting the suspension on a NEXTERION® ultra-clean glass B (Schott). An ultra-clean NEXTERION® glass cover slip (Schott) was put over the drop and sealed with adhesive tape to avoid oil penetration inside the sample. The measurements were carried out with a Xe 75W light source, and a 60x/1.25 oil lens.

Transmission electron microscopy (TEM)

The fine particles morphology and structure were analyzed by a transmission electron microscopy (TEM) using a JEOL, model JEM 2100 equipment, operating with a LaB_6 electron emitting filament, with a maximum acceleration voltage of 200 kV, using a drop casting technique in a copper grid (ultra-thin carbon Type-A; Ted Pella) and drying with neither fast nor slow evaporation.

Vibrating sample magnetometer (VSM)

Magnetic hysteresis curves were obtained using a vibrating sample magnetometer manufactured by EG&G Princeton Applied Research, model 4500, using magnetic fields of up to 20 kOe (2 Tesla - saturation field). The electromagnet used was produced by Walker Scientific - HR8 model. The Gauss meter was manufactured by Lake Shore - model 450.

X-ray fluorescence spectroscopy (EDXRF)

The X-ray fluorescence spectra (EDXRF) were obtained in 25 ºC in a Shimadzu EDX Model EDX-720, with Rh tube as a light source, 15-50 kV voltage, current varying from 1 to 1000 uA and Si (Li) semiconductor detector cooled in liquid nitrogen. The samples were analyzed as a power placed onto Mylar® films in a sample holder with 30 mm of diameter. To analyze the content of every particle, the samples were "opened" with a HCl/H_2O_2 or HF solution when needed.

Infrared spectroscopy (FTIR)

Infrared spectroscopy was recorded on an ALPHA Bruker FTIR spectrometer (KBr pellets, 96 scans) by a transmission/reflectance mode.

RESULTS AND DISCUSSION

The microtubules were initially examined using a dark-field Cytoviva™ hypermicroscope system. For this purpose, unlabeled tubulin was polymerized as previous described, placed into the flow cell and imaged with the microscope (Figure 3a, b). Visualization of microtubes requires passivating the glass surfaces (e.g., by flushing 20 µL of 0.5 mg/mL casein) to eliminate surface adsorption and hence polymer degradation. However, the "floating" of the microtubules along the z plane inside the flow cell decreased the quality of the optical images.

Cytoviva™ observation of unlabeled microtubules has proved very hard regardless of the many parameters tested in both microtubule polymerization and microscopic image acquisition. Therefore, to confirm whether microtubules were being rightly produced with correct laboratory expertise, unlabeled tubulin

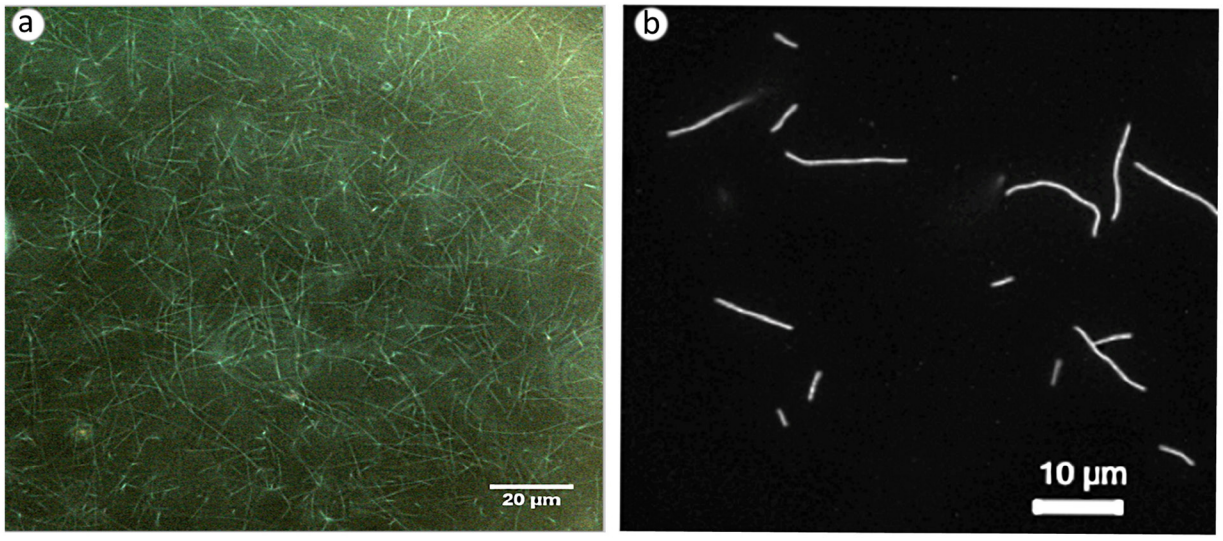

Figure 3. Images of unlabeled microtubules using the dark-field Cytoviva™ microscope (a), and of rhodamine labeled microtubules using the inverted fluorescence microscope (b).

was replaced by rhodamine-tagged tubulin. Observation of microtubules is overwhelmingly studied through fluorescent techniques and because of the difficulty to observe them with the Cytoviva™ method, fluorescence microscopy was the most straightforward technique to test whether microtubules were indeed being formed. As previously stated, a mixture of unlabeled tubulin and rhodamine-labeled tubulin (7:3) was used and allowed to polymerize for 30 min at 37 °C, yielding fluorescent microtubules. The fluorescence microscope images of the microtubules, measured in a flow cell, can be seen in Figure 3b. The microtubules appear bright and well-defined, exhibiting non-uniform lengths of tens of micrometers.

To further investigate polymerized microtubules, no test other than the gliding motility assay, can give information whether microtubules are, in fact, functional and active. The gliding motility assay is an experimental way to observe the motion of microtubule filaments over kinesin proteins. The experiment was performed as follows: kinesin stock vial was thawed and diluted in BRB80 buffer with 10 mM MgATP. Polymerized taxol-stabilized microtubules were diluted 10-fold in BRB80 buffer including 10 mM MgATP and 10 µM Taxol. For stable and long-lasting fluorescence observation, rhodamine-label microtubules were stabilized by adding mercaptoethanol (0.5 % (v/v)) and an anti-fade solution (20 µg/mL glucose oxidase, 8 µg/mL catalase, 20 mM glucose in BRB80 buffer). The glass surfaces of the flow cell were exposed to kinesin molecules by introducing 20 µL of kinesin solution (0.2 mg/mL kinesin, 10 mM ATP in BRB80 buffer) into the flow cell. The flow cell was then incubated at room temperature for 5 min. Next, 20 µL of the prepared microtubule solution was introduced into the flow cell to flush the chamber out and to fill it with the new solution. Finally, the kinesin-coated cell containing microtubules was sealed with nail polish and placed under the microscope for observations.

For the optimal functionality of the kinesin proteins in microtubule gliding assays, casein is typically employed to pretreat glass surfaces (Gramlich et al. 2017). However, it has been observed that inclusion of casein can suppress

the binding of microtubules to the kinesin surface. For this reason, in the present work, another alternative way of surface passivating (Liu et al. 2011) has been adopted, using a high surface density of kinesin molecules to cover the glass surface.

In Figure 4 one can see three fluorescence microscope images for a single microtubule filament taken at three subsequent times, with 15 s increments. As expected, the portrayed fluorescent microtubule really moved along the 30 s time interval. The microtubule gliding speed was calculated using the ZEN© software (Carl Zeiss™) by counting the number of pixels in the time-elapsed images (Figure 4a, b, c). The observed speed of 750 nm/s is slightly lower than the previously reported, i.e. 966 nm/s (Maloney et al. 2011). However, it should be noted that any precise comparison of gliding speed is not pertinent, since the published speed was obtained with casein as the passivating agent, contrasting with the high density of kinesin approach used here.

After confirming by fluorescence microscopy that the employed laboratory skills were successfully yielding stable and functional microtubules, the research focus moved into labeling them with superparamagnetic nanoparticles. The scope was to align the microtubules according to the magnetic field lines, creating controllable pathways for gliding the molecular machines.

The first step for achieving this was synthesizing the magnetic nanoparticles. As a regular procedure for working with biological systems (Netto et al. 2011), our laboratory has traditionally applied a silica coating by the controlled hydrolysis of TEOS over the Fe_3O_4 core for preventing its exposure to the chemical environment, and also helping to proceed with further functionalization, e.g. with APTS. The TEM/HRTEM of as-prepared nanoparticle is shown in

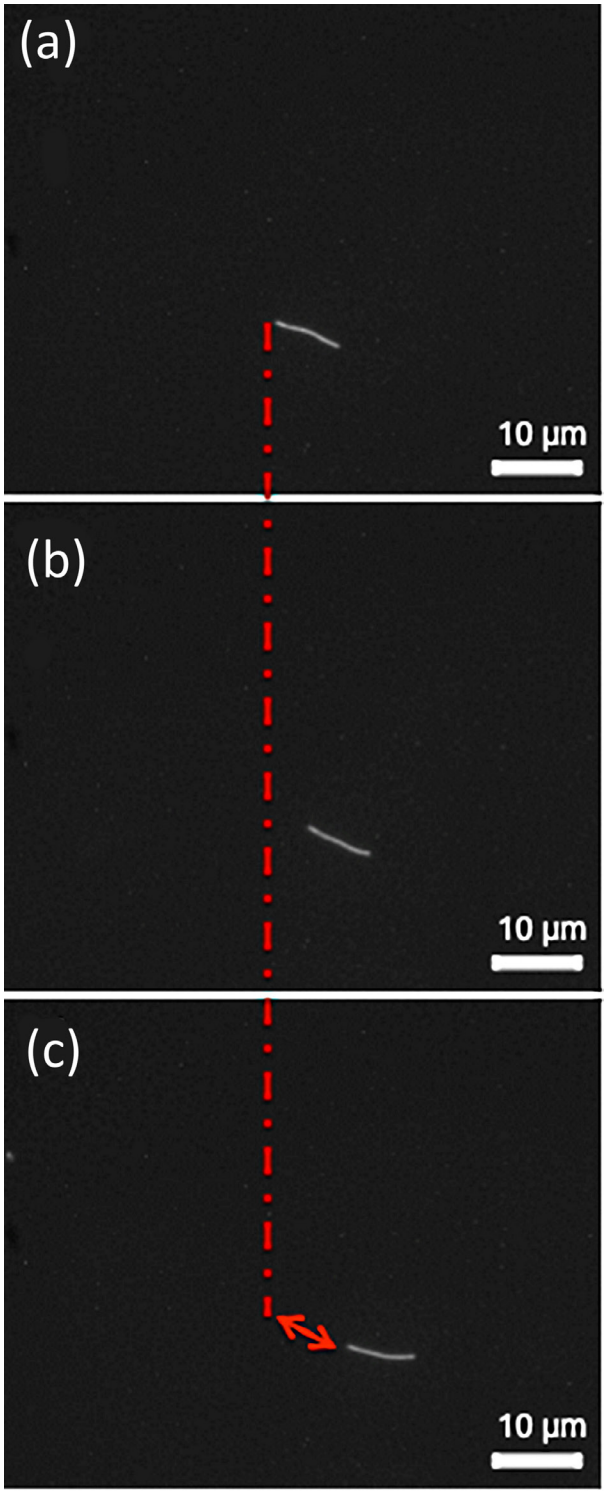

Figure 4. Time-elapsed (in seconds) microtubule gliding over kinesin (a) 0 s, (b) 15 s, and (c) 30 s.

Figure 5d. The nanoparticles present a regular spherical shape with a statistical mean size of 9,2 ± 1,3 nm (200 nanoparticles count). To confirm the presence of silanes at the nanoparticles surface, it was employed infrared spectroscopy and X-ray fluorescence spectroscopy. As one can see in Figure 5a, a new Si-O stretching peak arises after the recovering with silica that came from the hydrolysis of TEOS. In Figure 5b it is possible to see the Ka Si signal, confirming the presence of the silica protection. After applying the APTS coating (Yamaura et al. 2004) the particles become suitable for functionalization with SA (via glutaraldehyde cross-linking), to be used as a strong binding species to the biotin-labeled microtubules (Murray et al. 2000), (Boles et al. 2016), (Bruchez et al. 1998).

Figure 5c shows that the nanoparticles respond with a superparamagnetic behavior. It should be noted that in small particles the magnetic domain size becomes more uniform, leading to a strong increase in the coercivity. In

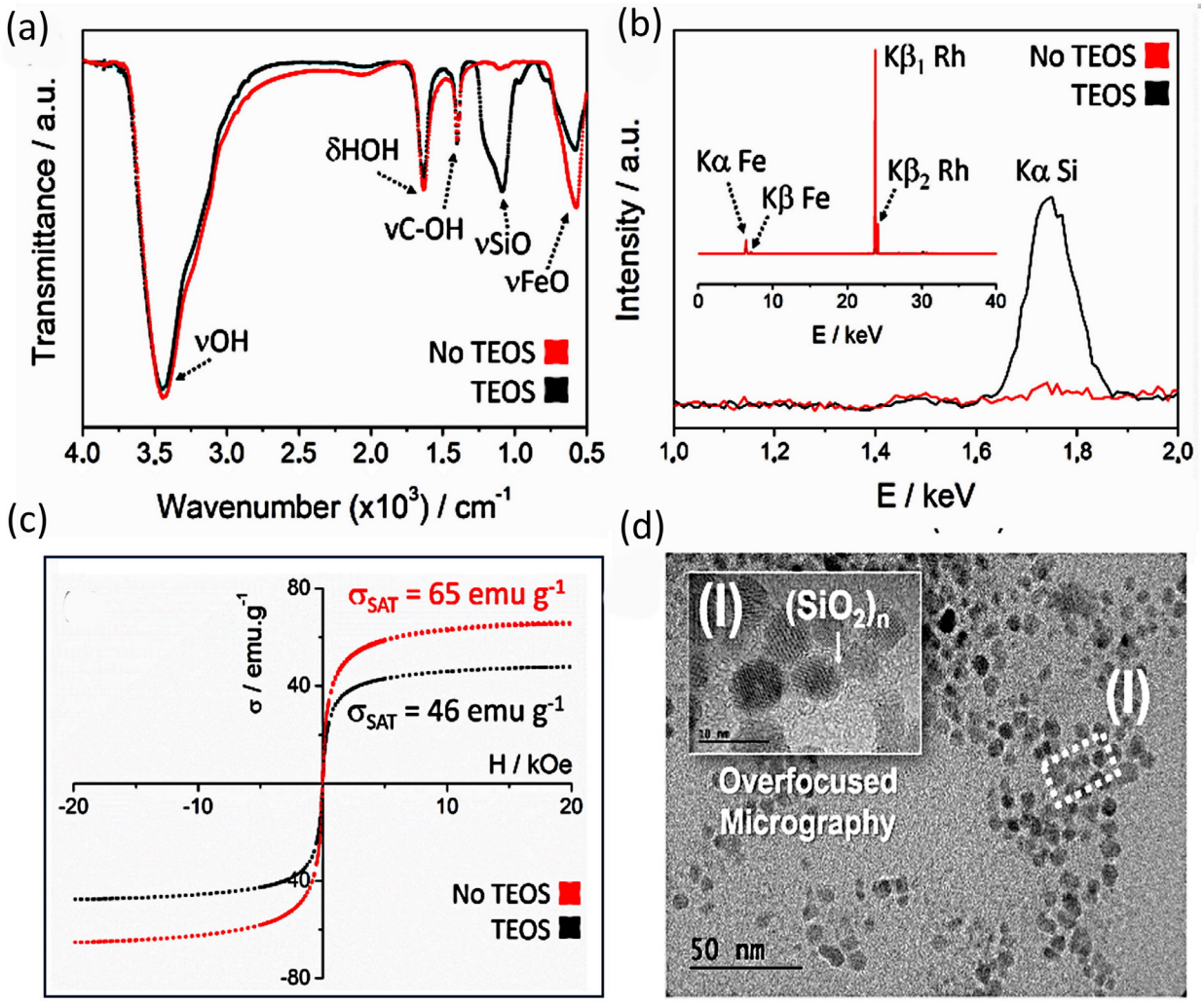

Figure 5. (a) FTIR of the as-prepared iron oxide nanoparticles before and after the silane functionalization (TEOS). **(b)** EDXRF analysis highlighting the Ka signals of Si, Fe and the lamp (Rh). **(c)** VSM measurement before and after the silanization process. **(d)** TEM micrography of MagNPs; Inset (I): Overfocused HRTEM image of MagNPs highlighting an amorphous surface probably due to the presence of silane polymer $(SiO_2)_n$.

the superparamagnetic state, the thermal energy overcomes the magnetostatic energy, resulting in zero hysteresis. After the silanization process, the saturation magnetization apparently decreases because the magnetic momentum is normalized by the total mass of the sample (considering Fe_3O_4 core and $(SiO_2)_n$ shell), (Melo et al. 2021), (Mathew et al. 2007).

The next step was co-polymerizing the rhodamine- and biotin-labeled microtubules. Rhodamine moieties would allow fluorescence imaging, while biotin moieties would mediate MagNPs functionalization through biospecific interaction with the nanoparticles SA layer. Accordingly, the labeling with SA-MagNPs was carried out by incubating with the rhodamine and biotin co-polymerized microtubules for 20 minutes. Then, a casein solution was injected into the flow cell and kept for 10 minutes. After that, the nanoparticle-functionalized microtubules were introduced, and the flow cell was placed in the fluorescence microscope for observation. In sequence, a neodymium magnet (1.1 T) was properly placed below the flow cell, and images of magnetic-labeled microtubules were taken, as shown in Figure 6, at three different locations. It should be noted that in the arrangement adopted, the magnet position is fixed while the position of the flow cell can be varied. This setup allows to acquire images at different spatial regions of the flow cell. In Figure 6 (a, b, c) the yellow arrow represents the magnetic field orientation relative through the flow cell along x axis, while the two white arrows indicate the coordinates.

As one can see, the microtubule images in Figures 6 (a,c) confirm their alignment and orientation in the magnetic field, confirming the validity of the proposed strategy. The possibility of controlling the microtubule orientation in the magnetic lines is indeed stimulating, but the next step, investigating the kinesin motion will be even more challenging. Currently it is not possible to predict the impact of the microtubule modifications on the molecular machine performance.

CONCLUSION

An experimental strategy has been tested in this work, with excellent results, for simultaneously monitoring the microtubules by fluorescence microscopy, and performing their controlled alignment in a magnetic field. Accordingly, the co-polymerization of the microtubes was initially performed by incubating a tubulin mix consisting of 7 biotinylated-tubulins to 3 rhodamine-tubulins. Such procedure proved efficient for introducing rhodamine as the fluorescent tag, and for adding biotin as the

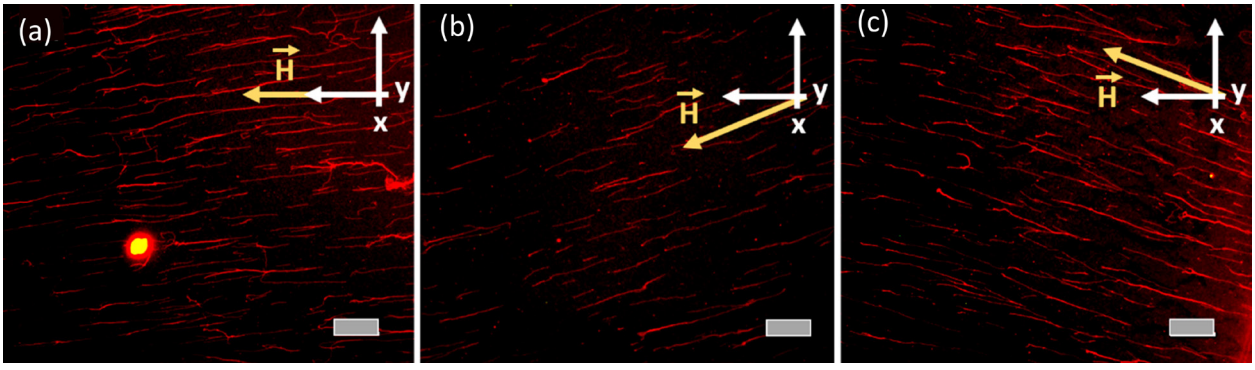

Figure 6. Magnetic-labeled microtubules fluorescence images under an applied magnetic field at 3 different positions (a, b, c) along the flow cell (indicated along x axis). The magnetic field direction is displayed as an yellow arrow. (Scale bar: 20 nm; Magnetic field: 1.1T).

anchoring group to streptavidin containing species. To accomplish the task, suitable superparamagnetic nanoparticles were synthesized, bearing streptavidin groups for attaching to the fluorescent microtubules. In this way, dual-labeled microtubules could be successfully generated, allowing their monitoring on an inverted fluorescence microscope, using a flow cell, in the presence of a magnetic field. Confirming the proposed strategy, the alignment and orientation of the magnetic-tagged microtubules has been demonstrated, illustrating a possible route for manipulating the biological structures involved in the cellular machinery.

Acknowledgements

The authors gratefully acknowledge Prof. Mauricio S. Baptista for providing the fluorescence microscopy facilities, and the financial support from Fundação de Amparo à Pesquisa do Estado de São Paulo (FAPESP) (2015/01271-3, 2018/21489-1).

REFERENCES

BACHAND GD, RIVERA SB, BOAL AK, GAUDIOSO J, LIU J & BUNKER BC. 2004. Assembly and transport of nanocrystal CdSe quantum dot nanocomposites using microtubules and kinesin motor proteins. NANO Lett 4: 817-821.

BOHM KJ, STRACKE R, MUHLIG P & UNGER E. 2001. Motor protein-driven unidirectional transport of micrometer-sized cargoes across isopolar microtubule arrays. Nanotechnol 12: 238-244.

BOLES MA, LING D, HYEON T & TALAPIN DV. 2016. The surface science of nanocrystals. Nat Mater 15: 141-153.

BROWN TB & HANCOCK WO. 2002. A polarized microtubule array for kinesin-powered-nanoscale assembly and force generation. NANO Lett 2: 1131-1135.

BRUCHEZ M, MORONNE M, GIN P, WEISS S & ALIVISATOS AP. 1998. Semiconductor nanocrystals as fluorescent biological labels. Science 281(80): 2013-2016.

CRICK FHC. 1950. The physical properties of cytoplasm. A study by means of the magnetic particle method. Part II. Theoretical treatment. Exp Cell Res 1: 505-533.

DA SILVA DG, TOMA SH, DE MELO FM, CARVALHO LVC, MAGALHAES A, SABADINI E, DOS SANTOS AD, ARAKI K & TOMA HE. 2016. Direct synthesis of magnetite nanoparticles from iron(II) carboxymethylcellulose and their performance as NMR contrast agents. J Magn Magn Mater 397: 28-32.

DINIZ K, DUTRA RS, PIRES LB, VIANA NB, NUSSENZVEIG HM & MAIA NETO PA. 2019. Negative optical torque on a microsphere in optical tweezers. Opt Express 27: 5905.

DIXIT R, ROSS JL, GOLDMAN YE & HOLZBAUR ELF. 2008. Differential regulation of dynein and kinesin motor proteins by tau. Science 319: 1086-1089.

DOOT RK, HESS H & VOGEL V. 2007. Engineered networks of oriented microtubule filaments for directed cargo transport. Soft Matter 3: 349-356.

DU YZ, HIRATSUKA Y, TAIRA S, EGUCHI M, UYEDA TQP, YUMOTO N & KODAKA M. 2005. Motor protein nano-biomachine powered by self-supplying ATP. Chem Commun 16: 2080-2082.

FISCHER T, AGARWAL A & HESS H. 2009. A smart dust biosensor powered by kinesin motors. Nat Nanotechnol 4: 162-166.

GRAMLICH MW, CONWAY L, LIANG WH, LABASTIDE JA, KING SJ, XU J & ROSS JL. 2017. Single Molecule Investigation of Kinesin-1 Motility Using Engineered Microtubule Defects. Sci Rep 13(7): 44290.

HUTCHINS BM, PLATT M, HANCOCK WO & WILLIAMS ME. 2006. Directing Transport of CoFe2O4-functionalized Microtubules with Magnetic Fields. Small 3(1): 126-131.

INABA H, YAMADA M, RASHID MR, KABIR AMR, KAKUGO A, SADA K & MATSUURA K. 2020. Magnetic Force-Induced Alignment of Microtubules by Encapsulation of CoPt Nanoparticles Using a Tau-Derived Peptide. Nano Lett 20(7): 5251-5258.

KATRUKHA EA, MIKHAYLOVA M, VAN BRAKEL HX, HENEGOUWEN PM VAN BE, AKHMANOVA A, HOOGENRAAD CC & KAPITEIN LC. 2017. Probing cytoskeletal modulation of passive and active intracellular dynamics using nanobody-functionalized quantum dots. Nat Commun 8: 1472.

KIRCHWINCK JL. 1994. Rock magnetism linked to human brain magnetite. Eos (Washington. DC) 178-179.

KEYA JJ, KABIR AR & KAKUGO A. 2020. Synchronous operation of biomolecular engines. Biophys Rev 12(2): 401-409.

LIU L, TUEZEL E & ROSS JL. 2011. Loop formation of microtubules during gliding at high density. J Physics-Condensed Matter 23: 374104.

MALONEY A, HERSKOWITZ LJ & KOCH SJ. 2011. Effects of Surface Passivation on Gliding Motility Assays. PLoS ONE 6: e19522.

MATHEW DS & JUANG RS. 2007. An overview of the structure and magnetism of spinel ferrite nanoparticles and their synthesis in microemulsions. Chem Engin J 129: 51.

MELO FM, GRASSESCHI D, BRANDÃO BBNS, FU Y & TOMA HE. 2018. Superparamagnetic Maghemite-Based CdTe Quantum Dots as Efficient Hybrid Nanoprobes for Water-Bath Magnetic Particle Inspection. ACS Appl Nano Mat 1: 2858-2868.

MELO FM, MATTIONI JV, DIAS F, FU Y & TOMA HE. 2021. Solvophobic-controlled synthesis of smart magneto-fluorescent nanostructures for real-time inspection of metallic fractures. Nanoscale Adv 3: 3593-3604.

MOORJANI SG, JIA L, JACKSON TN & HANCOCK WO. 2003. Lithographically patterned channels spatially segregate kinesin motor activity and effectively guide microtubule movements. NANO Lett 3: 633-637.

MURRAY CB, KAGAN CR & BAWENDI MG. 2000. Synthesis and characterization of monodisperse nanocrystals and close-packed nanocrystal assemblies. Annu Rev Mater Sci 30: 545-610.

NETTO CGCM, NAKAMATSU EH, NETTO LES, NOVAK MA, ZUIN A, NAKAMURA M, ARAKI K & TOMA HE. 2011. Catalytic properties of thioredoxin immobilized on superparamagnetic nanoparticles. J Inorg Biochem 105: 738-744.

NUSSENZVEIG HM. 2018. Cell membrane biophysics with optical tweezers. Eur Biophys J 47: 499-514.

NUSSENZVEIG HM. 2019. Are cell membrane nanotubes the ancestors of the nervous system? Eur Biophys J 48: 593-598.

OLADIPO A, COWAN A & RODIONOV V. 2007. Microtubule motor ncd induces sliding of Microtubules in vivo. Mol Biol Cell 18: 3601-3606.

OLIVEIRA D, DE MELO FM & TOMA HE. 2018a. One-pot single step to label microtubule with MPA-capped CdTe quantum dots. Micron 108: 19-23.

OLIVEIRA D, KIM DM, UMETSU M, KUMAGAI I, ADSCHIRI T & TEIZER W. 2012. The assembly of kinesin-based nanotransport systems. J Appl Phys 112: 124703.

OLIVEIRA D, SHINOHARA JD & TOMA HE. 2018b. Gold nanoparticle conjugation with microtubules for nanobiostructure formation. J Bionanoscience 12: 271-277.

OZEKI T, VERMA V, UPPALAPATI M, SUZUKI Y, NAKAMURA M, CATCHMARK JM & HANCOCK WO. 2009. Surface-Bound Casein Modulates the Adsorption and Activity of Kinesin on SiO2 Surfaces. Biophys J 96: 3305-3318.

PLATT M, MUTHUKRISHNAN G, HANCOCK WO & WILLIAMS ME. 2005. Milimeter Scale Alignment of Magnetic Nanoparticle Functionalized Microtubules in Magnetic Fields. JACS 2005(127): 15686-15687.

PÓSFAI M, LEFÈVRE CT, TRUBITSYN D, BAZYLINSKI DA & FRANKEL RB. 2013. Phylogenetic significance of composition and crystal morphology of magnetosome minerals. Front Microbiol 3: 344.

RATH O & KOZIELSKI F. 2012. Kinesins and cancer. Nat Rev Cancer 12: 527-539.

STOBER W, FINK A & BOHN E. 1968. Controlled grow of monodisperse silica spheresin micron size range. J Colloid Interface Sci 26: 62.

SMITH YJ, AGARWAL A & HESS H. 2010. Cargo loading onto kinesin powered molecular shuttles. J Vis Exp 45: 1-4.

UCHIYAMA MK ET AL. 2015. Ultrasmall cationic superparamagnetic iron oxide nanoparticles as nontoxic and efficient MRI contrast agent and magnetic-targeting tool. Int J Nanomedicine 10: 4731-4746.

VAINRUB A, PUSTOVYY O & VODYANOY V. 2006. Resolution of 90 nm (λ/5) in an optical transmission microscope with an annular condenser. Opt Lett 31: 2855.

VALE RD & MILLIGAN RA. 2000. The Way Things Move: Looking Under the Hood of Molecular Motor Proteins. Science 288: 88-95.

VAN DEN HEUVEL MGL & DEKKER C. 2007. Motor proteins at work for nanotechnology. Science 317: 333-336.

VANGIJZEGEM T, STANICKI D & LAURENT S 2019. Magnetic iron oxide nanoparticles for drug delivery: applications and characteristics. Expert Opin Drug Deliv 16: 69-78.

VAUTHIER C, TSAPIS N & COUVREUR P. 2011. Nanoparticles: heating tumors to death? Perspective 6: 99-109.

VERHEY KJ, KAUL N & SOPPINA V 2011. Kinesin assembly and movement in cells. Annu Rev Biophys 40: 267-288.

YAMAURA M, CAMILO RL, SAMPAIO LC, MACEDO MA, NAKAMURA M & TOMA HE. 2004. Preparation and characterization of (3-aminopropyl) triethoxysilane-coated magnetite nanoparticles. J Magn Magn Mater 279: 210-217.

How to cite
TOMA HE, OLIVEIRA D & DE MELO FM. 2022. Magnetic alignment of rhodamine/magnetite dual-labeled microtubules probed with inverted fluorescence microscopy. An Acad Bras Cienc 94: e20210917. DOI 10.1590/0001-3765202220210917.

Manuscript received on June 30, 2021;
accepted for publication on October 17, 2021

HENRIQUE EISI TOMA
https://orcid.org/0000-0002-4044-391X

DANIEL OLIVEIRA
https://orcid.org/0000-0002-9585-7503

FERNANDO M. DE MELO
https://orcid.org/0000-0003-0270-5912

Universidade de São Paulo, Instituto de Química,
Av. Prof. Lineu Prestes, 748, Cidade Universitária,
05508-000 São Paulo, SP, Brazil

Correspondence to: **Henrique Eisi Toma**
E-mail: henetoma@iq.usp.br

Author contributions

Daniel Oliveira performed the microtubules experiments and the microscopy work, Fernando Menegatti de Melo carried out the magnetic nanoparticles synthesis, characterization and writing the manuscript and Henrique Eisi Toma was responsible for supervising the project, and writing the manuscript.